Cell wall extension results in the coordinate separation of parallel microfibrils: evidence from scanning electron microscopy and atomic force microscopy

Francoise Marga[1,†], Michel Grandbois[2,‡], Daniel J. Cosgrove[3] and Tobias I. Baskin[1,*,§]

[1]*Division of Biological Sciences, University of Missouri, 109 Tucker Hall, Columbia, MO, 65211 USA,*

[2]*Department of Physics, University of Missouri, Columbia, MO, 65211 USA, and*

[3]*Department of Biology, Pennsylvania State University, 208 Mueller Lab, University Park, PA, 16802 USA*

Summary

Enlargement of the cell wall requires separation of cellulose microfibrils, mediated by proteins such as expansin; according to the multi-net growth hypothesis, enlargement passively reorients microfibrils. However, at the molecular scale, little is known about the specific movement of microfibrils. To find out, we examined directly changes in microfibril orientation when walls were extended slowly *in vitro* under constant load (creep). Frozen-thawed cucumber hypocotyl segments were strained by 20–30% by incubation in pH 4.5 buffer or by incubation of heat-inactivated segments in α-expansin or a fungal endoglucanase (Cel12A). Subsequently, the innermost layer of the cell wall was imaged, with neither extraction nor homogenization, by field-emission scanning electron microscopy (FESEM) and atomic force microscopy (AFM). AFM images revealed that sample preparation for FESEM did not appreciably alter cell wall ultrastructure. In both FESEM and AFM, images from extended and non-extended samples appeared indistinguishable. To quantify orientational order, we used a novel algorithm to characterize the fast Fourier transform of the image as a function of spatial frequency. For both FESEM and AFM images, the transforms of non-extended samples were indistinguishable from those of samples extended by α-expansin or Cel12A, as were AFM images of samples extended by acidic buffer. We conclude that cell walls *in vitro* can extend slowly by a creep mechanism without passive reorientation of innermost microfibrils, implying that wall loosening agents act selectively on the cross-linking polymers between parallel microfibrils, rather than more generally on the wall matrix.

Keywords: expansin, cel12A endoglucanase, fast Fourier transform, elongation, cell wall creep, *Cucumis sativus*.

Introduction

The cell wall of a growing plant cell must satisfy two contradictory requirements. The wall must be strong enough to resist the mechanical forces generated by cell turgor pressure and at the same time it must be sufficiently compliant to permit irreversible wall expansion. The cell wall accommodates these requirements through its composite structure, having stiff structural elements with high mechanical strength in series with plastic or viscous elements that move in a controlled fashion. In the growing wall, the stiff elements are the cellulose microfibrils while the cell wall matrix

constitutes viscous elements (Carpita and Gibeaut, 1993; Cosgrove, 2001). The microfibrils are long, crystalline ribbons composed of approximately 36 parallel chains of unbranched 1 → 4 linked β-D-glucan; microfibrils have a tensile strength similar to that of steel, and are inert and inextensible. When the cell wall expands, its microfibrils slip (shear) within the plane of the wall as a result of turgor-driven yielding (creep) of the compliant matrix. The matrix consists of cellulose-binding polysaccharides (hemicelluloses) that form a load-bearing network with cellulose

microfibrils, as well as hydrophilic pectic polysaccharides and structural proteins elaborated around the microfibril scaffold. The unmet challenge is to relate the microscopic structure of these intertwined polymers to the macroscopic behavior of the growing cell wall.

Plant cells rarely enlarge isotropically; instead, they grow preferentially in a single direction. It was learned years ago that the cellulose microfibrils are aligned on average perpendicular to the direction of maximal expansion rate (Frey-Wyssling, 1953). The cellulose co-alignment gives the cell wall a mechanical anisotropy that translates into a deformation anisotropy. Perpendicular to the direction of net microfibrillar alignment, elongation is facilitated, while parallel to the microfibrils, elongation is restrained (Green, 1980; Taiz, 1984). In cylindrical organs such as stems or coleoptiles, expansion is almost entirely in length, as well as rapid and sustained, and this type of material has been the subject of the majority of studies on the mechanism of elongation.

A detailed understanding of cell elongation requires a detailed understanding of the movement of cellulose microfibrils. Typically, the growing cell wall is represented as a multi-layer structure of approximately parallel microfibrils tethered or otherwise anchored by hemicelluloses, usually xyloglucan. When the tethers are broken down or remodeled, the microfibrils are imagined to be free to separate, resulting in cell elongation (Carpita and Gibeaut, 1993; Passioura, 1994). The image of parallel microfibrils tethered by polysaccharide strands is widely reproduced; nevertheless, it has seldom been tested explicitly.

We realized that the tethered-microfibril model predicts that agents that promote elongation should promote the parallel separation of microfibrils, without longitudinal reorientation. This prediction contrasts with other ideas and data about microfibril orientation. A long-standing and well accepted view of microfibril behavior is the multi-net growth model, which holds that, as the cell elongates, microfibrils rotate passively, becoming progressively aligned toward the long axis (except those that are precisely transverse). Passive rotation based on multi-net growth explains the observation that growing cells deposit microfibrils on the inner surface of the cell wall in a transverse orientation whereas the outer layers of the cell wall have more random or even longitudinal microfibrils (Gertel and Green, 1977; Green, 1960; Preston, 1982; Roelofsen, 1965). Furthermore, passive reorientation of microfibrils due to strain has been observed directly in bacterial cellulose composites (Astley et al., 2003) and in onion epidermis (Wilson et al., 2000), although both examples pertain to non-growing material and used rapid extensions rather than creep (slow, irreversible extension under constant force).

The tethered-microfibril model for growth is popular but is not the only possibility (Cosgrove, 2001). An important alternative model applies to ordinary composite materials, such as fiberglass, where the relevant interaction is between a fiber and its surrounding matrix (Probine and Preston, 1962; Talbott and Ray, 1992). Recently, for growing potato tubers, this type of model underlay a successful explanation of cell wall mechanical properties as quantified in transgenic plants synthesizing aberrant pectin (Ulskov et al., 2005). Therefore, the applicability of the tethered microfibril model remains an open question.

To address this question, our approach has been to image the cell wall at high resolution for samples that have, and have not, been extended slowly, under constant tension, mimicking the extension that occurs during growth (Cosgrove, 1989). We used this creep assay on non-living material because the continued deposition of microfibrils in a living cell makes it difficult to follow reorientation. We used the etiolated cucumber hypocotyl, whose large cells facilitate imaging and whose behavior in creep assays has been well characterized and related to *in vivo* elongation (Cosgrove, 1989). To induce creep, we used acidic pH, α-expansin (Cosgrove et al., 2002), and the Cel12A endoglucanase (Yuan et al., 2001). If agents that cause creep selectively act on taut polymers tethering microfibrils, then the microfibrils should remain parallel as the cell wall deforms; on the other hand, if microfibrils are enmeshed in a matrix that deforms uniformly, passive reorientation in the longitudinal direction would be expected.

Unfortunately, the classic method for imaging ultrastructure, transmission electron microscopy, is ill-suited to cell walls because polysaccharides are erratically stained by heavy metals. As an alternative, field-emission scanning electron microscopy (FESEM) has recently been gaining in popularity (Carpita et al., 2001; Sugimoto et al., 2000; Vesk et al., 1996). FESEM combines the ease of sample preparation typical of the conventional SEM with the ultrastructural magnification range of the transmission electron microscope. However, FESEM usually requires dehydration and critical-point drying, both of which may cause artifacts. To investigate hydrated cell walls, researchers have turned to atomic force microscopy (AFM), which produces an image based either on the topography of the sample or on its compliance (Morris et al., 1999). AFM is well suited to image the cell wall at high-resolution, even when the cell wall is submerged (Pesacreta et al., 1997).
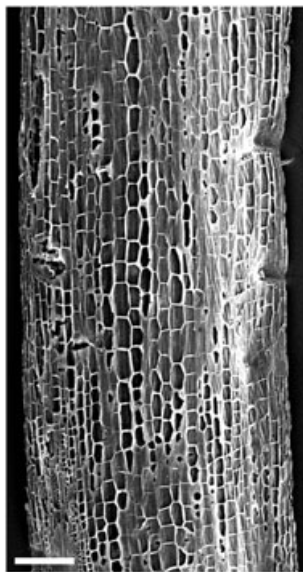
We report here, based on consistent FESEM and AFM images, that microfibril orientation is scarcely affected by *in vitro* extension (strains of 20–30%). This result is inconsistent with the expectations of passive realignment of microfibrils during multi-net growth; in contrast, the result agrees with models that posit cell wall loosening, hence elongation, results from specific loosening of selective stress-bearing polymers that link parallel microfibrils.
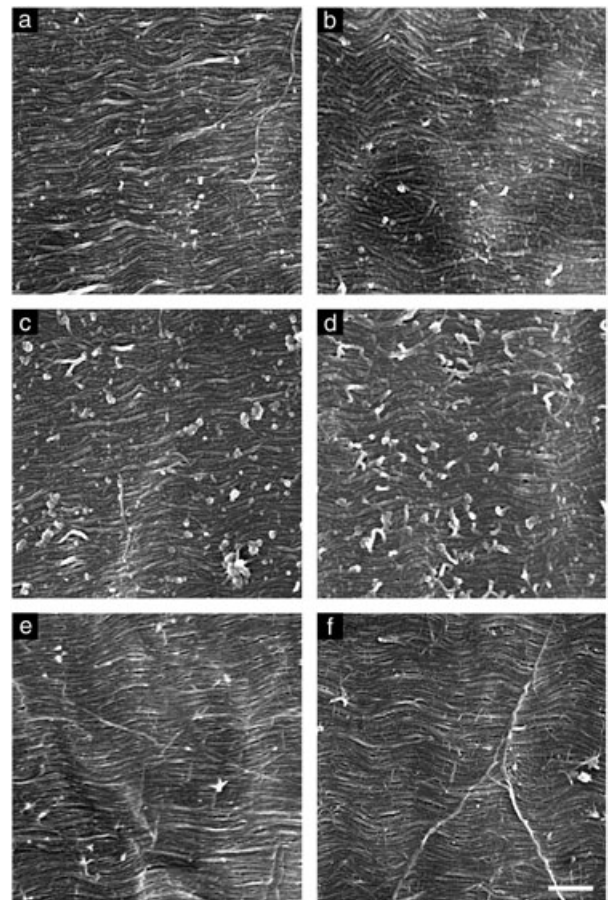
Results

Cell wall ultrastructure observed by FESEM

After cucumber hypocotyls are bisected and incubated in buffer, cell contents and the plasma membrane were lost completely from nearly all of the cells, and neither extraction nor bleach treatment was needed to expose cell wall microfibrils (Figure 1). At high magnification in FESEM, the cell wall had a well ordered fibrillar texture, with globular inclusions and apparent cross-links (Figure 2). The fibers were on average perpendicular to the long axis of the hypocotyl and are presumably cellulose microfibrils, enveloped by polysaccharides and proteins. The density of particulates adhering to the surface varied, being abundant in some samples (Figure 2c,d) and rare in others (Figure 2e,f); however, the variation seemed to be correlated to the day of the experiment rather than to treatment. Particulates were not removed by detergent rinses prior to fixation (data not shown).

The appearance of samples that had undergone considerable extension *in vitro* (creep) was indistinguishable from samples that had not (Figure 2, un-extended samples are on the left). This was true whether creep was induced in native cell walls by acidic buffer (Figure 2a,b), or (in heat-inactivated cell walls) by the addition of α-expansin (Figure 2c,d) or of the Cel12A endoglucanase (Figure 2e,f). Microfibrils appeared similarly transverse and undulated to about the same extent. Likewise, the texture of the native (not heat-inactivated) cell walls incubated at pH 6.8 (Figure 2a) resembled that of the heat-inactivated but un-extended cell

Figure 2. High-resolution FESEM images of the cell wall before (left) and after (right) extension promoted by acidic buffer (a, b), α-expansin (c, d) or Cel12A (e, f). Long axis of the hypocotyl is parallel to the long axis of the page. Scale bar = 200 nm.
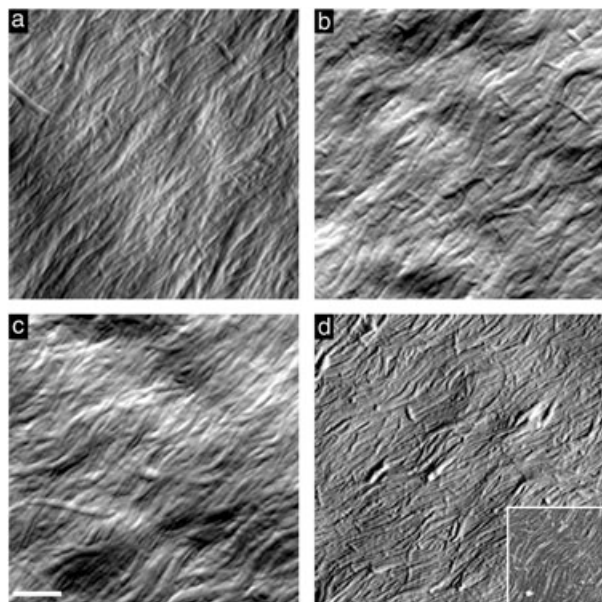
walls (Figure 2c,e). Given that the strain during extension was in the range of 20–30% of the initial length, the absence on any detectable change in ultrastructure is striking.

Cell wall ultrastructure observed by AFM

Because dehydration and critical-point drying may cause artifacts (Boyde, 1978; Bray *et al.*, 1993), changes in ultrastructure caused by creep might have been hidden by changes caused by sample preparation. Therefore, we imaged cell walls with AFM, which does not require dehydration or other harsh treatment. In the bisected hypocotyls, we were unable to image cell walls in water or buffer. However, samples could be removed from buffer, mounted, and imaged at once. As the cell wall binds water strongly and the underlying cells were intact and wet, we consider cell walls imaged in this way to be essentially fully hydrated but we will refer to such cell walls as 'partially hydrated' to indicate they are not submerged. A similar conclusion was made

Figure 1. Low magnification FESEM micrograph of a cucumber hypocotyl prepared for a creep experiment. Note how the cut opened cells have lost their contents and the longitudinal cell walls are exposed. Scale bar = 0.3 mm.

previously for AFM imaging of cell wall fragments (Kirby et al., 1996).

The AFM images of partially hydrated cell walls were consistent with a network of cellulose microfibrils oriented perpendicular to the elongation axis (Figure 3a). As in FESEM images, inclusions and potential cross-links were visible. Scanning the tip at 45° to the transverse provided the best image contrast, and is reflected in the oblique orientation of the microfibrils in the figures. A comparable organization was observed after fixation with 4% paraformaldehyde (Figure 3b) and after dehydration up to 50% ethanol (Figure 3c). Samples could not be imaged from 100% ethanol nor after critical-point drying, perhaps because of some interaction between the tip and mobile polymers at the cell wall surface. However, after sputter coating with platinum (exactly as for the FESEM preparation), the cell wall was readily imaged with AFM (Figure 3d). The coating flattened the image but the fibrillar texture was clear. The diameter of the fibrils of the coated samples was evidently smaller than that of the hydrated samples, but similar to the FESEM image (Figure 3d – inset). Except for fibril diameter, the appearance of the cell wall in the coated samples was not detectably different from the fresh, fixed, or partly dehydrated samples. Consequently, no support is offered for a major structural alteration in the cell walls induced by sample preparation for FESEM.

We then used AFM to determine whether *in vitro* extension affects cell wall ultrastructure. As for the FESEM images, samples had somewhat different overall appearance on different occasions, but no consistent differences were detected between extended and non-extended samples, whether creep was caused by acidic buffer (Figure 4a,b), α-expansin (Figure 4c,d), or the endoglucanase (Figure 4e,f; un-extended samples on the left).

Quantitative analysis of the images from extended versus un-extended cell walls

To extend the results beyond visual inspection, we developed a new algorithm, implemented in Image-J, to quantify the orientation of structures in the wall from the fast Fourier transform (FFT) of the image (described in Experimental procedures). The method analyses the elliptical shape of the transform as a function of frequency: the more eccentric the

Figure 3. AFM deflection images of the cell wall after the different steps for FESEM processing.
(a) Incubation in PBS.
(b) Fixation in 4% paraformaldehyde followed by rinsing in PBS.
(c) Dehydration to 50% ethanol.
(d) Complete FESEM processing, i.e. dehydration to 100% ethanol, critical point drying, and coating with platinum.
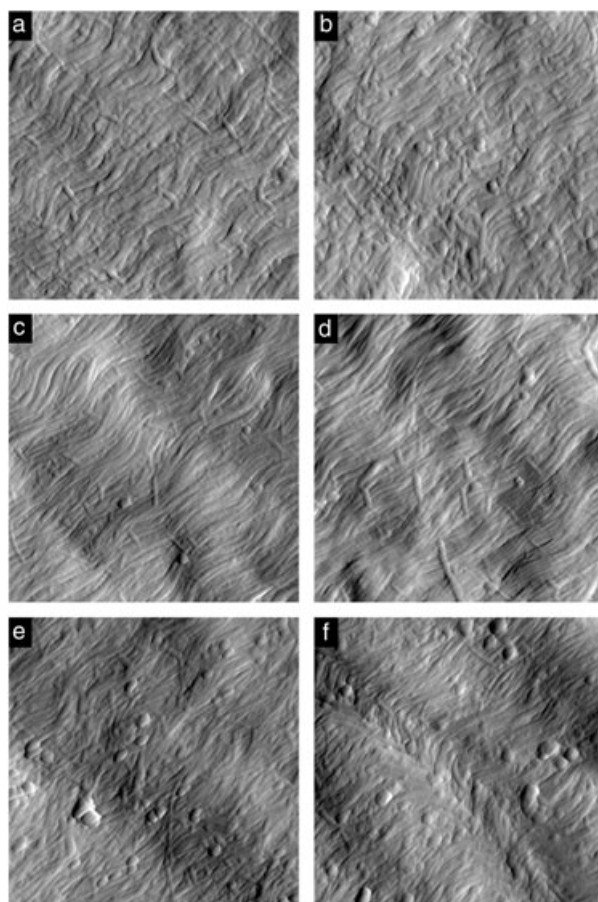The inset in (d) shows an FESEM image of the same section at about the same magnification. Long axis of the hypocotyl runs from upper left to lower right at 45° to the long axis of the page. Panels (b) and (c) were scanned at 3.5 μm × 3.5 μm and enlarged and cropped to match the 1.5 μm × 1.5 μm scans shown in (a) and (d). All scans at 2 Hz. Scale bar = 250 nm.

Figure 4. AFM deflection images of the cell wall before (left) and after (right) extension promoted by acidic buffer (a, b), α-expansin (c, d) or Cel12A (e, f). Long axis of the hypocotyl runs from upper left to lower right at 45° to the long axis of the page. All scans are 1 Hz, 1.5 μm × 1.5 μm.
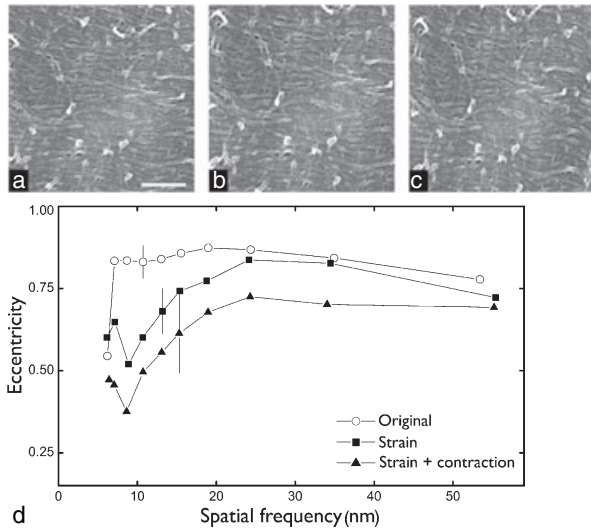
Figure 5. Computational creep.
(a) Original FESEM image.
(b) Image extended by 20%.
(c) Image extended by 20% and contracted so as to preserve image area. Note, (a–c) show square subsamples taken after image manipulation.
(d) FFTs of a set of eight images were analyzed by our routine, as described in 'Experimental procedures', and the average eccentricity plotted. The SD is shown at only a single point in each series for clarity. The size of the SD was essentially the same at all spacings but tended to be larger for the computationally extended images.

ellipse at a given frequency, the greater the orientational order at that frequency (with frequency in the transform corresponding to spacing in the image). To test whether our quantitative measure of orientation is sensitive to passive reorientation, we digitally manipulated images of cell walls to mimic wall extension with passive reorientation (Figure 5). Cell wall images that were 'computationally extended' by 20% displayed significantly lower eccentricity at most frequencies, confirming that our method is indeed sensitive to reorientation of image elements.

The eccentricity plots for AFM images of the real extended and un-extended samples were indistinguishable in all three treatments (Figure 6a–c). This confirms the visual impression that microfibrils do not passively realign toward the longitudinal direction during *in vitro* creep. The eccentricity plots for FESEM images likewise indicated that cell wall extension induced by α-expansin and Cel12A preserved microfibril orientation (Figure 6e,f). However, walls extended in acidic buffer and imaged with FESEM had less eccentric transforms than the un-extended walls (Figure 6d). This indicates that there was a reduction in the transverse orientation of wall structures during acid-induced extension of native cell walls, consistent with passive realignment. We note that the eccentricity (transverse orientation) of the control FESEM images was higher than for any other

Figure 6. Eccentricity of the FFT as a function of spacing. FFTs were analyzed by our routine, as described in 'Experimental procedures'. Symbols plot mean ± SE (some SE's are smaller than the symbol). The sharp rise at small spacings indicates the onset of meaningful signal in the FFT, and the onset at larger spacing for the AFM reflects the lower resolution of these images.
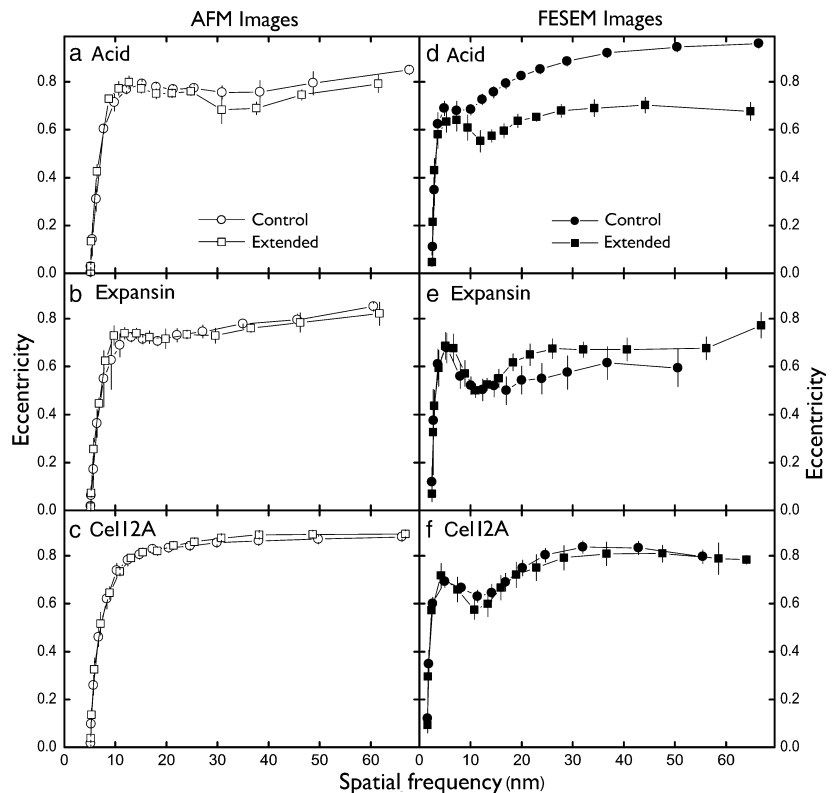
samples. Possibly, incubation of native walls in neutral pH stabilized or reinforced the transverse order; alternatively, heat inactivation and incubation at pH 4.5 induced some realignment of microfibrils. In any case, taken together, these quantitative analyses lead us to conclude that the cell wall can extend by up to 30% of its length without passive reorientation of wall microfibrils.

Discussion

To begin with, our studies examined the impact of *in vitro* extension (i.e. creep) on cell wall ultrastructure by means of FESEM. We found structural similarity between control and extended samples. Then, we verified this result by means of AFM on partially hydrated cell walls. Our results bear on methods for imaging the cell wall as well as on the mechanics of cell wall expansion.

The use of AFM to examine cell walls

In studies of cell walls, the atomic force microscope has been mainly used to characterize isolated macromolecules, and only a few investigators have imaged whole cell walls. Previous studies of primary cell walls mostly relied on extensive homogenization to prepare samples of the wall free of cytoplasm (Davies and Harris, 2003; Kirby *et al.*, 1996; Round *et al.*, 1996) or extracted all organic material except cellulose (van der Wel *et al.*, 1996). Cell wall images from these papers show microfibril textures that are considerably more disordered than shown here and often underlying lamellae are visible through gaps in the top lamella, whereas underlying lamellae were rarely if ever glimpsed here. It is possible that the difference reflects the source of tissue, insofar as the published AFM imaging has been done on parenchyma from non-growing tissues or callus, which may have a rather disorganized microfibril texture. Consistently, disorganized texture is seen in walls from non-growing parenchyma viewed as cryo-fixed, deep-etched replicas in the electron microscope, but highly parallel microfibrils are seen in elongating cells (McCann *et al.*, 1990). AFM images of microfibrils in cotton fibers, which have thick secondary-like cell walls, are also well ordered (Pesacreta *et al.*, 1997). On the other hand, homogenization of the cell wall to micron-sized pieces plausibly rearranges microfibrils to some extent. Furthermore, McCann *et al.* (1990) noticed that homogenization often shears the cell wall apart at its middle lamella and therefore some fragments might be imaged from the middle-lamella surface, which would be expected to be organized poorly.

Our approach uses a stem that had been bisected longitudinally but was otherwise intact, thus spared any potentially disruptive homogenization. To our knowledge, the cell wall in intact tissue has been imaged in high-resolution AFM in only one other study (Thimm *et al.*, 2000).

That study imaged celery collenchyma, exposed by peeling off the overlying epidermis and other tissues. These investigators were able to image the cell wall entirely submerged. The images are remarkable in that they show microfibrils in a perfectly parallel array, with neither undulation nor dispersion. Furthermore, when the cells were subjected to a dehydration in ethanol, the ordered texture became considerably disorganized. In contrast, we found microfibril textures that undulated and meandered, and dehydration was without effect on microfibril organization. Discovering reasons for the differences will require further study. We point out here that the use of organs simply cut and rinsed offers a gentle and easy way to expose the innermost layer of the cell wall for imaging, and when combined with the ability of the AFM to work in water should allow dynamic studies on the ultrastructural behavior of the native cell wall.

The use of FESEM to examine cell walls

FESEM has been used for many years to examine microfibril orientation in secondary cell walls (Abe *et al.*, 1991; Awano *et al.*, 2002; Hirakawa and Ishida, 1981), and is being used on primary cell walls with increasing frequency (Carpita *et al.*, 2001; Crow and Murphy, 2000; Sugimoto *et al.*, 2000; Vesk *et al.*, 1996; Wiedemeier *et al.*, 2002). Indeed, FESEM imaging has underpinned recent investigations on the role of microfibrils in controlling microfibril alignment and hence morphogenesis (Baskin *et al.*, 2004; Burk and Ye, 2002; Himmelspach *et al.*, 2003; Sugimoto *et al.*, 2003). The increasing popularity of FESEM results in part from the limitations of other methods. For example, transmission electron microscopy of sectioned material derives contrast from heavy metal stains that, unfortunately, do not stain polysaccharide components reliably (Emons, 1988; Erdos, 1986; McCann *et al.*, 1990). Transmission electron microscopy can be more appropriately used to image replicas of the cell wall made by coating samples with metal and carbon (e.g. Wolters-Arts and Sassen, 1991). Replicas have provided outstanding images of the cell wall (McCann *et al.*, 1990); however, they are difficult to prepare and the metal/carbon coat must be substantial because the sample is digested completely before observation. In contrast, FESEM images the cell wall directly and the coat needs to be thick enough only to make the sample conduct electrons.

Nevertheless, while preparing samples for FESEM is straightforward, the preparations customarily involve fixation, dehydration, and critical-point drying, any and all of which, in principle, could rearrange cell wall structure. Such concerns may be minimal for studies of wood where the microfibrillar network is presumably robust but are salient for the primary wall. Consequently, it has not been clear to what extent the previously published FESEM images of the primary cell wall reflect processing artifacts. Not only do the FESEM images obtained here resemble closely the images

of partially hydrated cell walls obtained by AFM, we could find no evidence in the AFM images that fixation, dehydration, or critical-point drying influenced the images to any appreciable extent. The lack of alteration is shown visually in Figure 3; moreover, processing sets of images from these steps through our FFT quantification routine failed to uncover any difference (data not shown).

A fundamental limitation of nearly all ultrastructural imaging methods is quantification. Beyond visual inspection, it is useful to compare images analytically. Toward that end, we have developed a method here to extract parameters based on orientation from the FFT. Ideally, the FFT would contain spots or arcs whose positions and dimensions were sufficiently clear to permit direct measurement (Russ, 1999). This would be the case for an image with nearly crystalline regularity; however, for the cell wall images obtained here, despite the human eye's assessment of order, the FFTs rarely if ever have defined spots. We surmounted this difficulty by fitting ellipses to the transforms at a series of steps defined by gray level, effectively sampling as a function of frequency. Our method is related to those published elsewhere for assessment of orientation (e.g. Tonar *et al.*, 2003).

Intriguingly, the eccentricity of the FFTs from the FESEM images for all treatments showed a peak for spacings of 3–5 nm (Figure 6). This is smaller than the fibrillar components obvious to the eye in the images (Figure 2), whose diameters are larger (15–20 nm) but close to the values reported for the diameter of single microfibrils in arabidopsis and onion (5.8 and 4.4 nm, respectively; Davies and Harris, 2003 and references therein). Under our conditions, this spacing was not resolved by the AFM so we cannot verify its presence by that method. This peak may reflect better organization among single microfibrils compared to larger structures or alternatively better organization of some unknown component of a similar size.

The invariance of cell wall structure to *in vitro extension*

The motivation underlying this work was to understand the polymer rearrangements that occur during cell wall extension. We used slow extension *in vitro* (i.e. creep) to examine extensions related to growth but without the complication of continued microfibril synthesis. During *in vitro* extension, the well accepted multi-net hypothesis predicts passive microfibril reorientation, whereas recent models of cell wall structure and growth predict an invariant cell wall structure. We found no evidence of passive reorientation of the innermost microfibrils. To verify the sensitivity of our quantification procedure, we performed a computational experiment. We took a set of FESEM images and stretched the images longitudinally (perpendicular to the net microfibril axis) by 20%, a value that is less than the experimental strains. Additionally, a second set of images was stretched

and also contracted by 20%, keeping cell wall area constant. The latter treatment presumably more closely mimics the actual creep assay, although the exact amount of contraction is not known. While the eye has difficulty seeing the distortions, the eccentricity plots clearly revealed the disorganization caused by these purely geometrical manipulations (Figure 5), demonstrating that our procedure has sufficient sensitivity to detect passive reorientation due to strain.

A potential explanation for our failure to see a consistent passive rearrangement of cell wall structure due to creep is that extended sections underwent a slow contraction after being released from the extensometer. There is an elastic contraction that occurs rapidly after un-loading but this is essentially the same magnitude for both extended and un-extended samples (D.J. Cosgrove, unpublished observations). As creep is a dissipative process, finding that segments contracted back to their original length would be more remarkable than invariant cell wall architecture. However, sensitive measurements of segment length for 5 h following unloading detected no significant contraction (D.J. Cosgrove and D.M. Durachko, unpublished data). Thus, cell wall creep was irreversible in these experiments.

Both expansin and Cel12A allowed segments to extend by as much as 30% of the initial length without causing a visible or quantifiable change in microfibril orientation. According to the multi-net theory, a strain of 30% is expected to rotate all microfibrils except those that are exactly transverse (Preston, 1982). Conceivably, the microfibrils have an exactly transverse orientation despite the undulations and hence would suffer little multi-net reorientation. This idea is contradicted by our 'computational creep' simulation (Figure 5). A more plausible explanation is that the loosening agents (expansin, Cel12A) specifically attack taut links between parallel microfibrils. This would tend to increase their spacing without reorienting them. Strikingly, in 1936, Bonner reported that stretching oat coleoptiles (with turgor eliminated through plasmolysis) changed the net orientation of microfibrils in cortical parenchyma from transverse to longitudinal at a strain of 8% unless the coleoptile had previously been treated with auxin, in which case a strain of 40% was needed. He argued explicitly that auxin promoted elongation by breaking taut bonds between parallel microfibrils. Likewise for oat coleoptiles, Morikawa *et al.* (1978) reported that auxin treatment minimized the strain-induced disorientation of microfibrils as assayed by dichroic absorption at specific infrared wavelengths.

In summary, our results demonstrate that the slow microfibril creep mediated by wall loosening agents such as α-expansin and Cel12A is distinctly different from that which occurs in rapid elastic and viscoelastic deformations, where passive reorientation occurs. In recent years, loosening bonds between parallel microfibrils has been implicit in molecular models of elongation, despite little direct justification. Now, to understand how plant cells regulate

elongation, we must understand how tension-bearing polysaccharides are distinguished from slack ones, and consequently selected as substrates for wall loosening and stress relaxation.

Experimental procedures

Extension measurement

Dark-grown cucumber (*Cucumis sativus* L.) seedlings were grown at 27°C on water-soaked germination paper (Kimpak K-22; Seedburo Equipment Co., Chicago, IL, USA) and harvested after 3 days. Hypocotyls were excised and stored at −20°C for up to a month before use. For experiments, an apical, approximately 1.5 cm segment (roughly encompassing the most active half of the growing region) was trimmed from the frozen hypocotyl, bisected longitudinally and thawed. For assays with α-expansin or the Cel12A endoglucanase, bisected segments were heat-inactivated in boiling water for 15 sec. All segments were pressed between glass slides under 500 g for 5 min, blotted dry, and clamped in the extensometer, and constant-load extension assays were carried out as described (Cosgrove, 1989). For buffer treatment of native (non-heat-inactivated) walls, bisected segments were incubated either in 50 mM HEPES, pH 6.8 (control) or in 50 mM sodium acetate, pH 4.5. For α-expansin or endoglucanase treatments, samples were incubated in 50 mM sodium acetate, pH 4.5, with or without addition of sufficient protein (5–10 μg active protein mL^{-1}) to cause rapid extension, approximately 10% h^{-1}. Creep experiments were carried out with each wall specimen in a cuvette containing approximately 150 μl of solution. After 2.5 h, samples were released, fixed in 4% paraformaldehyde in phosphate-buffered saline (PBS) buffer for 2 h at room temperature, and rinsed well in PBS. In separate experiments (data not shown), we confirmed that the wall extension was irreversible by monitoring the length of the wall sample after tension was released.

The α-expansin was extracted from cucumber hypocotyls and the Cel12A endoglucanase was purified from a *Trichoderma* enzyme preparation, as described by McQueen-Mason *et al.* (1992) and Yuan *et al.* (2001), respectively.

Microscopy

After fixation and rinsing as described for extension measurement, samples for FESEM were dehydrated in a graded ethanol series (approximately 45 min per step), 100% ethanol overnight, critical-point dried, mounted on stubs with double-sided carbon tape, sputter coated with platinum (approximately 2 nm), and examined in a Hitachi S4700 cold-cathode field-emission scanning electron microscope at 5 kV, with working distances between 5 and 7 mm. Samples for AFM, after fixation and rinsing, were attached to a holder with double-sided carbon tape and imaged in air on a Nanoscope III AFM. In some cases, samples were not fixed but simply bisected and rinsed in PBS. Highest contrast images were obtained when the scan angle of the tip was at 45° to the longitudinal axis of the hypocotyl. Measurements were performed in contact mode at a scan rate of 1 or 2 Hz. The AFM was fitted with silicon nitride triangular cantilevers (Sharp Microlever; Veeco Instruments Inc., Freemont, CA, USA) having a nominal spring constant of 0.01 N m^{-1} and used as provided.

For samples treated with acid buffer or α-expansin, a different set of samples was imaged for FESEM and AFM. For Cel12A-treated samples, treated hypocotyls were cut transversely with one half used for FESEM and the other for AFM.

Quantification of ultrastructure with the fast Fourier transform

The Fourier transform encodes spatial patterns in frequency space, containing information about both periodicity and orientation, and is thus a useful tool for characterizing the periodic properties of an image (Russ, 1999). However, while extremely regular objects give transforms that contain just a few peaks (frequencies), most objects typically have transforms without clear peaks and from which information is difficult to extract. For example, to the eye, the FE-SEM image of a cell wall appears well ordered, containing microfibrils of a roughly uniform diameter aligned horizontally with modest undulations; however, the Fourier transform has only a vaguely elliptical cloud of points (Figure 7a,b). While the long axis of the ellipse is perpendicular to the net alignment of the microfibrils, there are no spots or arcs in the transform corresponding to a pronounced periodicity, as would be produced by strictly uniform spacing between microfibrils (or strictly uniform microfibril diameter).

Orientation parameters were quantified from the FFT by means of a novel algorithm, implemented as a plug-in for Image-J (v. 1.31e; US National Institutes of Health; http://rsb.info.nih.gov/ij) by Chris Coulon (GAIA Group, Novato, CA, USA). In three dimensions (*x, y, I*), the FFT can be likened to a mountain, with contour levels linking frequencies represented equally in the image. The algorithm analyses the overall shape of the transform at a series of 'altitudes'. The more circular the shape, the less well oriented are the repeating
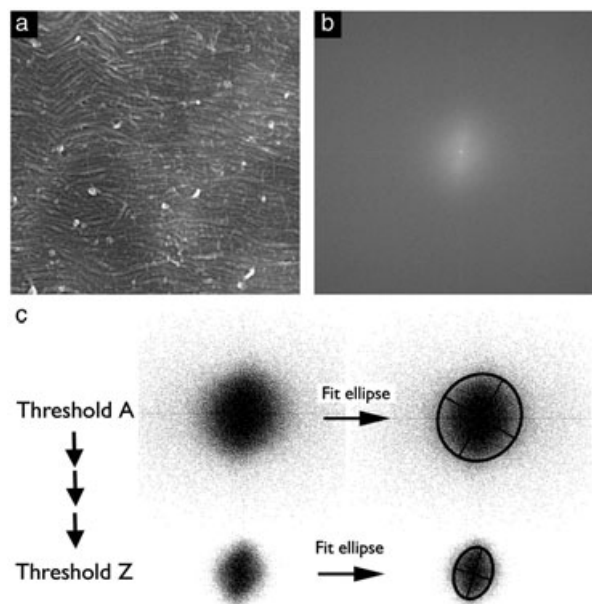
Figure 7. A routine to derive orientation parameters from the FFT.
(a) Starting image.
(b) Unprocessed FFT.
(c) Schematic of the routine.
A binary image is made of the FFT by choosing a threshold that includes most of the signal (cloud of black points); an ellipse is fit to the boundary and the major and minor axes are obtained analytically. The threshold is incremented by five gray levels (to whiter values) and a new ellipse fit. This is repeated until the area of the threshold is <200 pixels (smaller than shown). A parameter characterizing the shape of the ellipse, e.g. eccentricity, can then be plotted versus the average ellipse radius to characterize orientational order in the original image as a function of spacing.

structures at that altitude, i.e. frequency. To begin, an image region is selected and its FFT calculated (the FFT algorithm requires the selected region to be square). The transform was thresholded to generate a binary image, separating pixels containing power (black) from the background (white). An ellipse, a rough approximation to the shape of the transform, was fitted to the average boundary between black and white pixels, and the major and minor axes recorded as well as the angle between the major axis and the vertical (Figure 7c). The procedure started at the lowest threshold that gave a distinct shape, incremented the threshold by five gray levels, and stopped when the area of the black pixels contained <200 pixels. Eccentricity (*E*) was calculated from the major (*a*) and minor (*b*) axes as:

$$E = \frac{\sqrt{a^2 - b^2}}{a} \tag{1}$$

Eccentricity at each threshold was assigned to the frequency of an average ellipse radius $(a + b)/4$, and this frequency was converted to a distance by dividing it into the total width of the transform in pixels. Finally, the distance was calibrated by means of the image magnification.

For the analysis shown in Figure 6, FESEM images were captured at 2560×1920 pixel and FFTs obtained for three 512×512 pixel subsamples. The parameters from the three subsamples were averaged and used to represent that image. For acid and expansin, eight or nine images were captured in total from three different hypocotyls and plotted as mean for the images ± SE; for Cel12A, seven to 15 images were captured from each of four to five hypocotyls and plotted as the mean for the hypocotyls ± SE. AFM images were captured at 512×512 pixel and FFTs obtained for the entire image. For acid-buffer-treated samples, 12–19 images were captured from each of four hypocotyls; for α-expansin-treated samples, five to seven images were captured each from two or three hypocotyls; and for Cel12A-treated cell walls, six to 10 images were captured from each of four or six hypocotyls. Data are plotted as mean for the hypocotyls ± SE.

For the computational model of creep (Figure 5), a set of eight FESEM images were used that had been captured at 640×480 pixel resolution, manipulated digitally (in Adobe Photoshop, version 7, bi-cubic resampling) to mimic creep, and a single 256×256 pixel subsample used for FFT analysis.

Acknowledgements

References

Abe, H., Ohtani, J. and Fukazawa, K. (1991) FE-SEM observations on the microfibrillar orientation in the secondary wall of tracheids. *IAWA Bull.* **12**, 431–438.

Astley, O.M., Chanliaud, E., Donald, A.M. and Gidley, M.J. (2003) Tensile deformation of bacterial cellulose composites. *Int. J. Biol. Macromol.* **32**, 28–35.

Awano, T., Takebe, K. and Fujita, M. (2002) Xylan deposition on secondary wall of *Fagus crenata* fiber. *Protoplasma*, **219**, 106–115.

Baskin, T.I., Beemster, G.T.S., Judy-March, J.E. and Marga, F. (2004) Disorganization of cortical microtubules stimulates tangential expansion and reduces the uniformity of cellulose microfibril alignment among cells in the root of *Arabidopsis thaliana*. *Plant Physiol.* **135**, 2279–2290.

Bonner, J. (1936) Zum Mechanismus der Zellstreckung auf Grund der Micellarlehre. *Jahrb. Wiss. Bot.* **82**, 377–412.

Boyde, A. (1978) Pros and cons of critical point drying and freeze drying for SEM. *Scan. Electron Microsc.* **11**, 303–314.

Bray, D.F., Bagu, J. and Koegler, P. (1993) Comparison of hexamethyldisilazane (HMDS), Peldri II, and critical-point drying methods for scanning electron microscopy of biological specimens. *Microsc. Res. Tech.* **26**, 489–495.

Burk, D.H. and Ye, Z.-H. (2002) Alteration of oriented deposition of cellulose microfibrils by mutation of a katanin-like microtubule-severing protein. *Plant Cell*, **14**, 2145–2160.

Carpita, N.C. and Gibeaut, D.M. (1993) Structural models of primary cell walls in flowering plants: consistency of molecular structure with the physical properties of the walls during growth. *Plant J.* **3**, 1–30.

Carpita, N.C., Defernez, M., Findlay, K., Wells, B., Shoue, D.A., Catchpole, G., Wilson, R.H. and McCann, M.C. (2001) Cell wall architecture of the elongating maize coleoptile. *Plant Physiol.* **127**, 551–565.

Cosgrove, D.J. (1989) Characterization of long-term extension of isolated cell walls from growing cucumber hypocotyls. *Planta*, **177**, 121–130.

Cosgrove, D.J. (2001) Wall structure and wall loosening: a look backwards and forwards. *Plant Physiol.* **125**, 131–134.

Cosgrove, D.J., Li, L.C., Cho, H.-T., Hoffmann-Benning, S., Moore, R.C. and Blecker, D. (2002) The growing world of expansins. *Plant Cell Physiol.* **43**, 1436–1444.

Crow, E and Murphy, R.J. (2000) Microfibril orientation in differentiating and maturing fibre and parenchyma cell walls in culms of bamboo (*Phyllostachys viridiglaucescens* (Carr.) Riv. & Riv.). *Bot. J. Linn. Soc.* **134**, 339–359.

Davies, L.M. and Harris, P.J. (2003) Atomic force microscopy of microfibrils in primary cell walls. *Planta*, **217**, 283–289.

Emons, A.M.C. (1988) Methods for visualizing cell wall texture. *Acta Bot. Neerl.* **37**, 31–38.

Erdos, G.W. (1986) Localization of carbohydrate-containing molecules. In *Ultrastructure Techniques for Microorganisms* (Aldrich, H.C. and Todd, W.J., eds). New York: Plenum, pp. 399–420.

Frey-Wyssling, A. (1953) *Submicroscopic Morphology of Protoplasm*. Amsterdam: Elsevier, pp. 279–292.

Gertel, E.T. and Green, P.B. (1977) Cell growth pattern and wall microfibrillar arrangement. Experiments with *Nitella*. *Plant Physiol.* **60**, 247–254.

Green, P.B. (1960) Multinet growth in the cell wall of *Nitella*. *J. Biophys. Biochem. Cytol.* **7**, 289–296.

Green, P.B. (1980) Organogenesis – a biophysical view. *Ann. Rev. Plant Physiol.* **31**, 51–82.

Himmelspach, R., Williamson, R.E. and Wasteneys, G.O. (2003) Cellulose microfibril alignment recovers from DCB-induced disruption despite microtubule disorganization. *Plant J.* **36**, 565–575.

Hirakawa, Y. and Ishida, S. (1981) A SEM study on the layer structure of secondary wall of differentiating tracheids in conifers. *Res. Bull. College Exp. Forests Hokkaido Univ.* **38**, 55–71.

Kirby, A.R., Gunning, A.P., Waldron, K.W., Morris, V.J. and Ng, A. (1996) Visualization of plant cell walls by atomic force microscopy. *Biophys. J.* **70**, 1138–1143.

McCann, M.C., Wells, B. and Roberts, K. (1990) Direct visualization of cross-links in the primary plant cell wall. *J. Cell Sci.* **96**, 323–334.

McQueen-Mason, S., Durachko, D.M. and Cosgrove, D.J. (1992) Two endogenous proteins that induce cell wall extension in plants. *Plant Cell*, **4**, 1425–1433.

Morikawa, H., Kitamura, S. and Senda, M. (1978) Effect of auxin on changes in the oriented structure of wall polysaccharides in response to mechanical extension in oat coleoptile cell walls. *Plant Cell Physiol.* **19**, 1553–1556.

Morris, V.J., Kirby, A.R. and Gunning, A.P. (1999) *Atomic Force Microscopy for Biologists*. London: Imperial College Press.

Passioura, J.B. (1994) The physical chemistry of the primary cell wall: implications for the control of expansion rate. *J. Exp. Bot.* **45**, 1675–1682.

Pesacreta, T.C., Carlson, L.C. and Triplett, B.A. (1997) Atomic force microscopy of cotton fiber cell wall surfaces in air and water: quantitative and qualitative aspects. *Planta*, **202**, 435-442.

Preston, R.D. (1982) The case for multinet growth in growing walls of plant cells. *Planta*, **155**, 356–363.

Probine, M.C. and Preston, R.D. (1962) Cell growth and the structure and mechanical properties of the wall in internodal cells of *Nitella opaca*. II. Mechanical properties of the walls. *J. Exp. Bot.* **13**, 111–127.

Roelofsen, P.A. (1965) Ultrastructure of the wall in growing cells and its relation to the direction of the growth. *Adv. Bot. Res.* **2**, 69–149.

Round, A.N., Kirby, A.R. and Morris, V.J. (1996) Collection and processing of AFM images of plant cell walls. *Microsc. Anal.*, **55**, 33–35.

Russ, J.C. (1999) *The Image Processing Handbook*. Boca Raton, FL: CRC Press, pp. 305–370.

Sugimoto, K., Williamson, R.E. and Wasteneys, G.O. (2000) New techniques enable comparative analysis of microtubule orientation, wall texture, and growth rate in intact roots of arabidopsis. *Plant Physiol.* **124**, 1493–1506.

Sugimoto, K., Himmelspach, R., Williamson, R.E. and Wasteneys, G.O. (2003) Mutation or drug-dependent microtubule disruption causes radial swelling without altering parallel cellulose microfibril deposition in arabidopsis root cells. *Plant Cell*, **15**, 1414–1429.

Taiz, L. (1984) Plant cell expansion; regulation of cell wall mechanical properties. *Annu. Rev. Plant Physiol.* **35**, 585–657.

Talbott, L.D. and Ray, P.M. (1992) Molecular size and separability features of pea cell wall polysaccharides. Implications for models of primary wall structure. *Plant Physiol.* **98**, 357–368.

Thimm, J.C., Burritt, D.J., Ducker, W.A. and Melton, L.D. (2000) Celery (*Apium graveolens* L.) parenchyma cell walls examined by AFM: effect of dehydration on cellulose microfibrils. *Planta*, **212**, 25–32.

Tonar, Z., Němeček, S, Holota, R., Kočová, J., Třeška, V., Moláček, J., Kohoutek, T. and Hadravská, Š. (2003) Microscopic image analysis of elastin network in samples of normal, atherosclerotic and aneurysmatic abdominal aorta and its biomechanical implications. *J. Appl. Biomed.* **1**, 149–159.

Ulskov, P., Wium, H., Bruce, D., Jorgensen, B., Qvist, K.B., Skjøt, M., Hepworth, D., Borkhardt, B. and Sørensen, S.O. (2005) Biophysical consequences of remodeling the neutral side chains of rhamnogalacturonan I in tubers of transgenic potatoes. *Planta*, **230**, 609–620.

Vesk, P.A., Vesk, M. and Gunning, B.E.S. (1996) Field emission scanning electron microscopy of microtubule arrays in higher plant cells. *Protoplasma*, **195**, 168–182.

van der Wel, N.N., Putman, C.A.J., van Noort, S.J.T., de Grooth, B.G. and Emons, A.M.C. (1996) Atomic force microscopy of pollen grains, cellulose microfibrils, and protoplasts. *Protoplasma*, **194**, 29–39.

Wiedemeier, A.M.D., Judy-March, J.E., Hocart, C.H., Wasteneys, G.O., Williamson, R.E. and Baskin, T.I. (2002) Mutant alleles of arabidopsis *RADIALLY SWOLLEN 4* and *RSW7* reduce growth anisotropy without altering the transverse orientation of cortical microtubules or cellulose microfibrils. *Development*, **129**, 4821–4830.

Wilson, R.H., Smith, A.C., Kacuráková, M., Saunders, P.K., Wellner, N. and Waldron, K.W. (2000) The mechanical properties and molecular dynamics of plant cell wall polysaccharides studied by Fourier-transform infrared spectroscopy. *Plant Physiol.* **124**, 397–405.

Wolters-Arts, A.M.C. and Sassen, M.M.A. (1991) Deposition and reorientation of cellulose microfibrils in elongating cells of petunia stylar tissue. *Planta*, **185**, 179–189.

Yuan, S., Wu, Y. and Cosgrove, D.J. (2001) A fungal endoglucanase with plant cell wall extension activity. *Plant Physiol.* **127**, 324–333.